

Fossil and genomic evidence constrains the timing of bison arrival in North America

Duane Froese^{a,1}, Mathias Stiller^{b,c}, Peter D. Heintzman^b, Alberto V. Reyes^a, Grant D. Zazula^d, André E. R. Soares^b, Matthias Meyer^e, Elizabeth Hall^d, Britta J. L. Jensen^{a,f}, Lee J. Arnold^g, Ross D. E. MacPhee^h, and Beth Shapiro^{b,i,1}

^aDepartment of Earth and Atmospheric Sciences, University of Alberta, Edmonton, AB, Canada T6G 2E3; ^bDepartment of Ecology and Evolutionary Biology, University of California, Santa Cruz, CA 95064; ^cGerman Cancer Consortium, German Cancer Research Center, Institute for Translational Skin Cancer Research, D-45141 Essen, Germany; ^dYukon Palaeontology Program, Department of Tourism & Culture, Government of Yukon, Whitehorse, YT, Canada Y1A 2C6; ^eDepartment of Evolutionary Genetics, Max Planck Institute for Evolutionary Anthropology, 04103 Leipzig, Germany; ^fRoyal Alberta Museum, Edmonton, AB, Canada T5N 0M6; ^gSchool of Physical Sciences, Environment Institute, and Institute for Photonics and Advanced Sensing, University of Adelaide, Adelaide, SA 5005, Australia; ^hDivision of Vertebrate Zoology, American Museum of Natural History, New York, NY 10024; and ⁱUniversity of California, Santa Cruz Genomics Institute, University of California, Santa Cruz, CA 95064

Edited by Donald K. Grayson, University of Washington, Seattle, WA, and approved February 3, 2017 (received for review December 20, 2016)

The arrival of bison in North America marks one of the most successful large-mammal dispersals from Asia within the last million years, yet the timing and nature of this event remain poorly determined. Here, we used a combined paleontological and paleogenomic approach to provide a robust timeline for the entry and subsequent evolution of bison within North America. We characterized two fossil-rich localities in Canada's Yukon and identified the oldest well-constrained bison fossil in North America, a 130,000-y-old steppe bison, *Bison cf. priscus*. We extracted and sequenced mitochondrial genomes from both this bison and from the remains of a recently discovered, ~120,000-y-old giant long-horned bison, *Bison latifrons*, from Snowmass, Colorado. We analyzed these and 44 other bison mitogenomes with ages that span the Late Pleistocene, and identified two waves of bison dispersal into North America from Asia, the earliest of which occurred ~195–135 thousand y ago and preceded the morphological diversification of North American bison, and the second of which occurred during the Late Pleistocene, ~45–21 thousand y ago. This chronological arc establishes that bison first entered North America during the sea level lowstand accompanying marine isotope stage 6, rejecting earlier records of bison in North America. After their invasion, bison rapidly colonized North America during the last interglaciation, spreading from Alaska through continental North America; they have been continuously resident since then.

Beringia | *Bison latifrons* | *Bison priscus* | paleogenomics | Rancholabrean | steppe bison

The invasion of bison (*Bison*) from Asia across the Bering Isthmus profoundly affected the North American faunal community. Bison, or American buffalo, are large-bodied, aggressive, and highly fecund. Following their establishment in North America, bison rapidly became the most important competitor for forage within the established large mammal community (1). Early North American bison were morphologically and ecologically diverse (2, 3). In addition to extant *Bison bison*, taxa traditionally recognized in systematic treatments include the steppe bison (*Bison priscus*), which first colonized northwestern North America from Asia, and the giant long-horned bison (*Bison latifrons*) of the central and southern continent (Figs. 1*A* and 2). The latter is the largest bison known. It inhabited woodlands and forest openings through much of the continental United States and southern Canada; however, their fossils have not been found in northern Canada or Alaska. Bison eventually became an important hunting resource for Indigenous North Americans (4) and remain an icon of the American plains (5).

At the time of bison arrival, the North American megaherbivore grazing community was dominated by mammoths (*Mammuthus*) and caballine equids (*Equus*). Equids have a deep evolutionary history in North America that is closely associated with the rise of grasslands during the Early Miocene (~18 Ma)

(6). Mammoths dispersed from Asia to North America during the Early Pleistocene (~1.35 Ma), becoming the continent's largest-bodied obligatory grazer (7). The subsequent arrival of *Bison* markedly affected a faunal community dominated by *Equus* and *Mammuthus*, but when that process actually began has been difficult to determine.

Paleontologically, *Bison* is the index taxon for the Rancholabrean, the final North American Land Mammal Age (8–10). Land Mammal ages are important because, in the absence of other chronological data, they provide a means to infer the age of a locality based on taxonomic assemblages. This assumes, however, that the first appearance datum of the index taxon can be reliably tied to a specific interval, which is surprisingly not the case for bison (8). Here, we used a combined paleontological and paleogenomic approach to establish the timing of bison entry into North America.

Models of the timing of *Bison* entry into North America range, based on fossil occurrences, from arrival during the Late Pliocene or Early Pleistocene, approximately 2–3 Ma, to the Late Pleistocene (8). The oldest of these dates are based on fossil sites in Florida (11) and Alaska (12) that have now been shown to be of poor stratigraphic and chronologic integrity (8, 13, 14). A bison astragalus dating to 290–230 thousand y before present (kyBP), or marine isotope stage (MIS) 7, was recovered from South Carolina (15), but the reliability of this age and its association with the fossils have also been questioned (16, 17). Bison fossils are absent in well-dated Middle Pleistocene (780–130 kyBP) localities from both central and northern North America (8). In

Significance

The appearance of bison in North America is both ecologically and paleontologically significant. We analyzed mitochondrial DNA from the oldest known North American bison fossils to reveal that bison were present in northern North America by 195–135 thousand y ago, having entered from Asia via the Bering Land Bridge. After their arrival, bison quickly colonized much of the rest of the continent, where they rapidly diversified phenotypically, producing, for example, the giant long-horned morphotype *Bison latifrons* during the last interglaciation.

Author contributions: D.F. and B.S. designed research; D.F., M.S., P.D.H., A.V.R., G.D.Z., A.E.R.S., M.M., E.H., B.J.L.J., L.J.A., R.D.E.M., and B.S. performed research; G.D.Z. and L.J.A. contributed new reagents/analytic tools; P.D.H., A.V.R., A.E.R.S., and L.J.A. analyzed data; and D.F., P.D.H., A.V.R., G.D.Z., M.M., L.J.A., R.D.E.M., and B.S. wrote the paper.

The authors declare no conflict of interest.

This article is a PNAS Direct Submission.

Data deposition: The sequences reported in this paper have been deposited in the GenBank database (accession nos. [KX269109](#), and [KX269112–KX269145](#)).

¹To whom correspondence may be addressed. Email: duane.froese@ualberta.ca or beth.shapiro@gmail.com.

This article contains supporting information online at www.pnas.org/lookup/suppl/doi:10.1073/pnas.1620754114/-DCSupplemental.

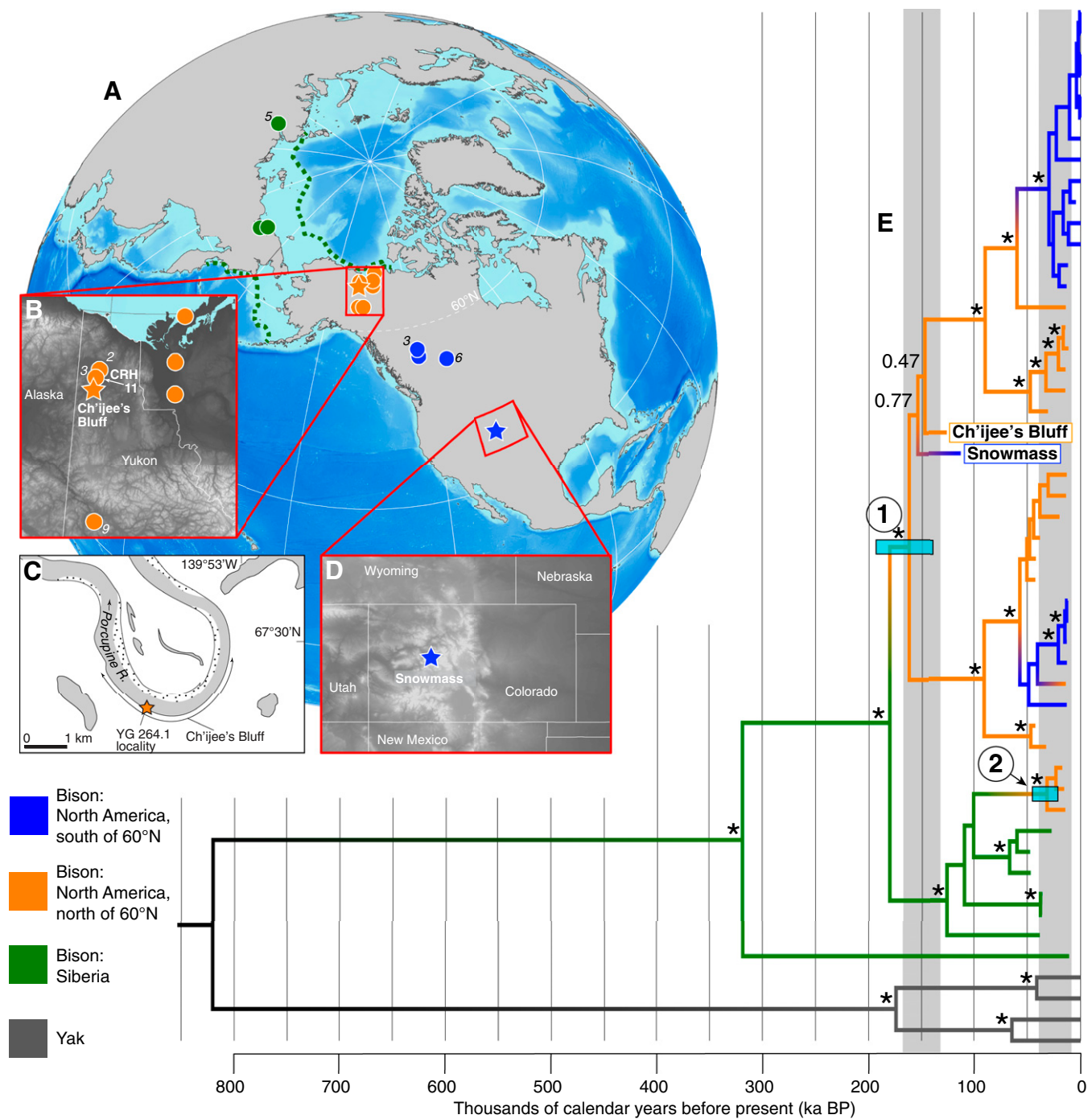


Fig. 1. (A) Localities of the 36 fossil bison. Siberia: green; North America north of 60° N: orange; North America south of 60° N: blue. The number of samples is given in italics if >one sample was recovered. The green dashed lines outline the last glacial maximum Bering Land Bridge extent. Insets showing locations of (B) CRH 11 (labeled orange circle) and Ch'ijee's Bluff (orange star) in northern Yukon, with (C) a zoom-in on Ch'ijee's Bluff, and (D) Snowmass, Colorado (blue star). (E) Bayesian phylogeny resulting from analysis of the reduced mitochondrial alignment, calibrated using the ages of the bison fossils from which data were generated. Nodes with posterior support of >0.99 are indicated with a black asterisk and other values are provided for deep nodes. The positions of the Ch'ijee's Bluff and Snowmass bison are highlighted. We identify two waves of dispersal from Asia into North America via the Bering Land Bridge (nodes 1 and 2), with date ranges indicated as light blue bars. Areas of gray shading indicate intervals of lowered sea level sufficient to expose the Bering Land Bridge (36).

Kansas, bison remains are all younger than the Lava Creek B Ash, which has a maximum constraining age of 640 kyBP (18). Bison fossils are also absent from the rich Sheridanian fauna “*Equus* beds” of Nebraska (19), which are overlain by the Loveland loess, dated regionally using optically stimulated luminescence to 180–130 kyBP, or MIS 6 (20). In Yukon, a fossil assemblage in stratigraphic association with the Middle Pleistocene

Gold Run tephra (735 ± 88 kyBP) includes horse (*Equus*), proboscideans (*Mammuthus*), sheep (*Ovis*), and biostratigraphically diagnostic microtine rodent species, but bison fossils are absent (21–23). The oldest site in the midcontinental United States possessing both bison and a firm chronology is near Snowmass, Colorado, where bison fossils were recovered within sediments associated with the last interglaciation (MIS 5d), thus dating to

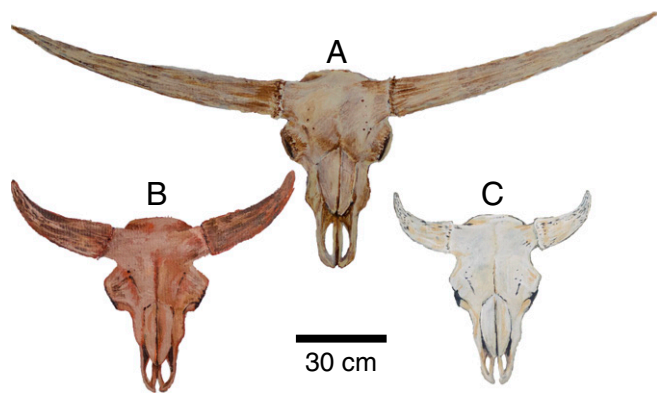


Fig. 2. Reconstructions of bison skulls based on fossils attributed to (A) a giant long-horned bison, *B. latifrons*; (B) a Late Pleistocene steppe bison, *B. priscus*; and (C) a present-day *B. bison*. Giant long-horned bison were significantly larger than present-day bison; adult males may have weighed in excess of 2,000 kg, which is twice as large as present-day bison, and had horns that spanned as much as 2.2 m (57, 58).

~120 kyBP (24). Bison fossils also occur at American Falls, Idaho, associated with a lava-dammed lake that dates to ~72 kyBP (8, 25). Bison from both of these sites represent the giant long-horned bison, *B. latifrons* (24, 25), generally considered to be the earliest form of bison developed in the continental United States.

To establish a reliable first appearance datum for bison in North America, we first characterized the in situ fossil assemblage and chronology of two, well-dated fossil-rich localities in the Old Crow area of northern Yukon, Canada: CRH 11 and Ch'ijee's Bluff (Figs. 1 B and C and 3). Next, we isolated and sequenced mitochondrial genomes from two of the oldest *Bison* fossils yet identified: a partial metacarpal found at Ch'ijee's Bluff that dates to ~130 kyBP (Fig. 3C), and a humerus from the site near Snowmass recovered within a layer dated to ~120 kyBP (Fig. 1D). These two bison were identified, based on their size and geographic location, as a steppe bison and a giant long-horned bison (24), respectively. We then used a coalescent-based approach to infer a mitochondrial genealogy for these and 44 other Late Pleistocene and Holocene bison, taking advantage of an approach to calibrate a molecular clock within a coalescent framework using the ages of each sampled bison (26).

This approach allows an estimate of the age of relevant nodes in the bison mitochondrial genealogy, making it possible to test hypotheses not only about the timing of bison entry into North America but also about the relationship between these morphologically distinct bison forms.

Results and Discussion

Characterizing Two Fossil Assemblages in Yukon, Canada. To assess the chronology of bison presence in high-latitude northwest North America, we first characterized the in situ fossil assemblage and chronology at CRH 11 (27, 28) and Ch'ijee's Bluff (Fig. 3). The chronologies of both of these sites rely heavily on identification of volcanic ash layers, or tephra, in sediment exposures. Individual tephra are readily characterized geochemically and, when combined with other correlative indicators—such as stratigraphy or paleoecology—can provide isochronous stratigraphic markers across a region (29). The Old Crow tephra has an isothermal plateau glass fission-track age of 124 ± 10 kyBP at the 1σ confidence level (29). This age determination spans the transition from the late MIS 6 glacial to the MIS 5e interglaciation, but paleoecological evidence for cool climate conditions during tephra deposition indicates a late MIS 6 age (29, 30). The Old Crow tephra thus provides a useful marker horizon for this study: interglacial deposits below the tephra must date to MIS 7 or older, whereas sediment above the tephra but below the prominent interglacial deposits represents a narrow time interval between latest MIS 6 and the beginning of MIS 5e (~135 to ~125 kyBP).

CRH 11 is one of the classic localities for Quaternary paleontology in North American Beringia. This bluff, on the left bank of the Old Crow River ($67^\circ 49' N$, $139^\circ 51' W$) comprises ~30 m of silt and sand that is locally organic-rich (28). We recovered 294 vertebrate fossils from the lowest bone-bearing unit at CRH 11, including specimens of woolly mammoth (*Mammuthus primigenius*), horse (*Equus* sp.), caribou (*Rangifer tarandus*), giant beaver (*Castoroides ohioensis*), beaver (*Castor canadensis*), wolverine (*Gulo gulo*), and Jefferson's ground sloth (*Megalonyx jeffersonii*) (for a complete list, see *SI Text*). *Bison* fossils are absent, consistent with earlier in situ assemblages recovered from the site (27). The Old Crow tephra is present 14 m above the in situ fossils (Fig. S1), establishing that the fossiliferous sediments must be older than the last interglaciation (pre-MIS 5e) and, based on paleoecology, date from the penultimate interglaciation, MIS 7 (28). To confirm this age, we performed direct single-grain optically stimulated luminescence dating of these sediments (*SI Text*),

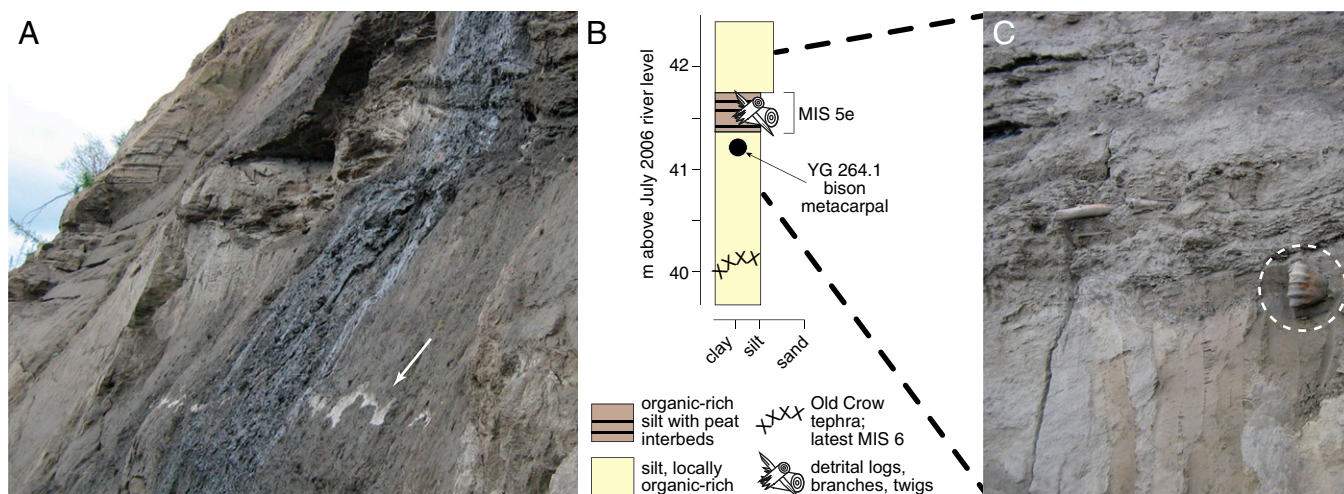


Fig. 3. Features of the Ch'ijee's Bluff locality. (A) the Old Crow tephra (124 ± 10 kyBP; UA1206) highlighted by the white arrow, (B) the stratigraphic setting of the Old Crow tephra, bison metacarpal YG 264.1, and the MIS 5e forest bed, and (C) the in situ metacarpal was found several centimeters beneath the prominent MIS 5e forest bed and ~125 cm above Old Crow tephra (the latter is not shown). The stratigraphy indicates a latest MIS 6 age for YG 264.1.

which gave a weighted mean age of 208 ± 6 kyBP (Figs. S2–S4), consistent with a MIS 7 age. Bison fossils were absent not only from this stratigraphic level at CRH 11, but also from nearby sites of comparable age (27), suggesting that bison were not present in Yukon before MIS 6.

Bison fossils are present, however, at nearby Ch'ijee's Bluff 40 km southwest ($67^{\circ} 29' N$, $139^{\circ} 56' W$), where 50 m of unconsolidated Late Cenozoic sediment are exposed along a prominent 4-km-long cut bank on the Porcupine River (Figs. 1C and 3). The Old Crow tephra (29) is present across much of Ch'ijee's Bluff (Fig. 3A), where it underlies a prominent bed of dark-brown macrofossil-rich organic silt. Paleocological indicators within this organic layer represent a closed boreal forest and a warmer than present climate, indicating a MIS 5e age (30, 31). In support of this age and the stability of the organic layer, logs and organic detritus from the organic bed all have nonfinite ^{14}C ages (30, 31). Although most bison fossils at the site are detrital, we recovered a single in situ bison metacarpal (YG 264.1) 125 cm above the Old Crow tephra and directly below the prominent MIS 5e woody peat bed (Fig. 3B and C). The tephra- and bone-bearing silt containing the fossil is sharply overlain by the organic-rich bed, an unconformity related to the thawing of permafrost during the last interglaciation that is common across northwestern Canada and Alaska (30). Given this stratigraphic context, we conclude that the bison fossil dates to ~ 130 kyBP: it is younger than late MIS 6 (the age of Old Crow tephra), and older than the onset of the MIS 5e interglaciation. This is the oldest reliably dated fossil evidence of bison in North America (cf. ref. 8).

The Oldest Fossil Bison in North America. Bison fossils are common throughout Yukon, Alaska, and Siberia. All are medium-horned bison, most commonly referred to as steppe bison, *B. priscus* (2), and published genetic data are consistent with this interpretation (3). The discovery of giant long-horned bison at a last interglacial site (MIS 5 *sensu lato*) near Snowmass, Colorado, establishes the presence of a morphologically distinct bison in continental North America (Fig. 2A). These giant long-horned forms have never been recovered from northern locales between Yukon and Siberia (2). The age of the Snowmass site places the long-horned bison fossil slightly younger than the bison from Ch'ijee's Bluff.

Because of their antiquity and the poor preservation conditions of continental compared with northern (permafrost) localities, giant long-horned bison fossils have thus far failed to yield usable DNA. However, recent advances in paleogenomics have expanded the range of fossils from which DNA can be recovered (32). Capitalizing on these, we used a hybridization capture approach to enrich for bison mitochondrial DNA from both the Ch'ijee's Bluff bison and from a giant long-horned bison from Snowmass (DMNH EPV.67609) that dates to the last interglaciation, ~ 120 kyBP (24). We recovered a complete mitochondrial genome (159 \times coverage) from the Ch'ijee's Bluff bison and a near-complete mitochondrial genome (6.6 \times mean coverage) from the Snowmass bison (*Materials and Methods*). We assembled complete mitochondrial genomes from an additional 6 Siberian and 26 North American bison ranging in age from ~ 0.4 –45 kyBP (*Dataset S1*). We then estimated the evolutionary relationship between these and 10 present-day American (33, 34) and an ancient Siberian bison (35), using stratigraphic ages and radiocarbon dates to inform the molecular clock (*Materials and Methods* and *SI Text*).

Both the Ch'ijee's Bluff bison and the Snowmass bison mitochondrial lineages fall near the root of sampled bison mitochondrial diversity, indicating that both bison were early descendants of the first bison dispersing into North America (Fig. 1E). North American bison share a common maternal ancestor 195–135 kyBP (Fig. 1E, node 1, *SI Text*, and Fig. S5), consistent with the MIS 6 glaciation (Fig. 1E), and precluding models for a significantly older bison presence in North America. This timing is coincident with an interval of reduced eustatic sea level that would have enabled interchanges across the Bering Isthmus (36, 37). We also identify a second, later dispersal of bison from Asia into North America during the Late Pleistocene,

~ 45 –21 kyBP (Fig. 1E, node 2, *SI Text*, and Fig. S5), within a period of lowered sea level during the last glaciation (36).

The Rancholabrean is the most recent of the North American Land Mammal Ages, and has long been defined by the presence of bison in continental records (9). However, Bell et al. (8) argued that this North American Land Mammal Age should only apply to localities or faunules recovered from south of 55° North. Their reasoning was that, given its proximity to the Bering Land Bridge and eastern Eurasia, the northern part of the continent required a distinct chronology because of the potential for faunal mixing. Our results, however, show temporal and genetic affinity between the arrival of bison in northwestern Canada and their dispersal further south. The close genetic relationship between maternal lineages found in the earliest northern bison and the earliest continental bison argues for a rapid expansion of bison across the continent in a period of approximately 20,000 y between late MIS 6 and MIS 5d. These records also demonstrate the rapid phenotypic change from northern forms of bison (e.g., *B. priscus*, *B. alaskensis*) found in Siberia through Yukon, to *B. latifrons* in the continental United States.

The integration of independent geochronological data with faunal collections and a molecular dating approach constrains the history and dynamics of bison dispersal into North America. These complementary approaches provide a remarkably consistent picture of this grazer as it entered the continent during the sea level lowstand accompanying MIS 6 and spread from Alaska through the continental United States. The rapid dispersal and success of bison in North America make a strong case for bison as an index taxon for the Rancholabrean at a continental scale. Although full nuclear genomic resources for bison are not yet available, these well preserved specimens will be important to future work to better understand the genetic basis for the remarkable phenotypic variability in early North American bison. Given their relatively shallow history and success in North American ecosystems, the entry of bison stands with human arrival as one of the most successful mammalian dispersals into North America during the last million years.

Materials and Methods

This section provides an overview of the methods of this study; full details can be found in *SI Text*.

Geochronology. Chronology at Ch'ijee's Bluff and CRH 11 relies on identification of tephra in sediment exposures and optically stimulated luminescence (OSL) dating. Old Crow tephra was identified based on stratigraphic position, glass shard morphology, and grain-discrete glass major element geochemistry. Glass geochemical analyses were by wavelength dispersive spectrometry on a JEOL 8900 electron microprobe at University of Alberta following Reyes et al. (38), with correlations confirmed by concurrent analyses of an Old Crow tephra reference sample (Fig. S1).

We obtained four samples for single-grain OSL dating from immediately above and below the lower fossil-bearing horizon at CRH 11. Samples were processed under safe (dim red) light conditions using standard procedures (39) to isolate refined quartz fractions. We performed equivalent dose (D_e) measurements on 1,800–2,400 individual quartz grains per sample using the experimental apparatus described by Arnold et al. (40) and the single-aliquot regenerative-dose procedure shown in Table S1. We considered 3–6% of the measured grain populations suitable for D_e determination after applying the SAR quality assurance criteria (41). D_e estimation over high dose ranges (>300 Gy) was well-supported by the single-grain dose saturation characteristics and dose-recovery test results (Figs. S2 and S3). The natural D_e datasets exhibited low overdispersion values (11–14%) and are dominated by experimental rather than field-related D_e scatter (42) (Fig. S4). We therefore calculated the final burial doses using the central age model (43). Dose rates were calculated using a combination of field γ -ray spectrometry (FGS), high-resolution γ -ray spectrometry (HRGS), and inductively coupled plasma-mass spectrometry (ICP-MS) (Table S2). To calculate the final OSL ages, we assumed that the measured radionuclide activities and present-day field water/organic contents prevailed throughout the burial period of these perennially frozen deposits. An uncertainty of 10% was assigned to long-term water and organic content estimates to accommodate minor variations during the burial periods.

DNA Extraction, Sequencing, and Mitochondrial Genome Assembly. We assembled mitochondrial genomes for 35 ancient bison, including the Ch'j'ee's Bluff steppe bison and a giant long-horned bison from a site near Snowmass, Colorado (24). Of these, 21 were not associated with any stratigraphic or age information, and were sent to accelerator mass spectrometry (AMS) radiocarbon dating facilities for dating using ultrafiltered collagen (Dataset S1). We extracted DNA from 23 ancient bison using silica-based methods optimized for recovery of ancient DNA (44, 45), and included in our dataset 12 previously extracted bison (Dataset S1, and references therein). We converted extracted DNA to either double-stranded (46) or single-stranded (47) Illumina-compatible libraries. Mitochondrial DNA molecules were enriched using biotinylated RNA baits based on either the bison mitochondrial genome (GenBank: NC_012346) or a 242 mammal mitochondrial genome reference panel (48). We sequenced enriched libraries on the Illumina MiSeq or HiSeq platforms using paired-end chemistry. Sequencing read pairs were merged and adapter trimmed in SeqPrep. Merged and remaining unmerged reads were mapped to the bison mitochondrial genome using either Burrows-Wheeler Aligner (BWA) (49) or the iterative short-read assembler, MIA (50). We collapsed PCR duplicates using either bam-rmdup or MIA. For consensus sequence calling, we required each position to have a minimum of 3× coverage and a base agreement greater than 67% (51). To evaluate DNA preservation in these oldest bison, we used mapDamage (52) to assess patterns of DNA fragmentation and cytosine deamination (Fig. S6). The resulting ancient mitochondrial genomes ranged in coverage from 6.6× to 898.4× (Dataset S1). The Ch'j'ee's Bluff steppe bison had an average fragment length of 54 bp and was sequenced to 159× coverage, with all bases called following consensus calling, as above. The Snowmass bison, which was much more poorly preserved (Fig. S6 D–F), had an average fragment length of 35 bp, with 5,596 missing bases following consensus calling.

Phylogenetic Analysis. We aligned mitochondrial genomes from the 35 ancient bison described above with previously published mitochondrial genomes from 10 present-day American bison (33, 34), an ancient Siberian bison (35), and 4 yaks (*Bos grunniens*). We then created two datasets for phylogenetic analysis: one comprising the complete mitochondrial genome (full dataset), and another limited to only those sites in the mitochondrial genome in which we were able to call a consensus base for the Snowmass bison (reduced dataset). We partitioned both alignments and selected appropriate models of molecular evolution using PartitionFinder (53), and

inferred the evolutionary relationships among the sampled mitochondrial lineages using BEAST v1.8.3 (54). Following model testing (SI Text), our final analyses assumed a strict molecular clock and the skygrid coalescent prior (55). We calibrated the molecular clock using median calibrated radiocarbon ages for each sampled mitochondrial genome, and sampled the ages of Ch'j'ee's Bluff and Snowmass bison using a mean and SD of 125 ± 4.5 kyBP and 124 ± 8.5 kyBP, respectively (56). For each analysis, we ran two Markov chain-Monte Carlo chains for 60 million iterations each, sampling priors and trees every 3,000 iterations, and discarding the first 10% as burn-in, and combining the remainder. We visually inspected log files for run convergence using Tracer and summarized the sampled trees using TreeAnnotator. Phylogenies presented in the text and SI Text are maximum clade credibility trees (Fig. 1E and Fig. S5).

Data Accessibility. Dataset S1 includes repository and radiocarbon accession details for all fossil specimens analyzed. The Ch'j'ee's Bluff steppe bison specimen, YG 264.1, is archived in the fossils collections of the Vuntut Gwitchin First Nation Government in Old Crow, Yukon. The giant long-horned bison specimen from the site near Snowmass, DMNH EPV.67609, is archived in the vertebrate paleontology collections of the Denver Museum of Natural History, Colorado. Mitochondrial genome sequences have been deposited in GenBank, with accession numbers KX269109, and KX269112–KX269145. Input BEAST files are available as Dataset S2.

ACKNOWLEDGMENTS. We thank Andrew Fields, Brandon Letts, Dan Chang, Joshua Kapp, and Amanda Hart for technical assistance; Ben J. Novak for the bison skull paintings in Fig. 2; Ian Miller, Joe Sertich, and the Denver Museum of Nature and Science for access to the Snowmass sample; and Harold Frost, Jr. and the late Stephen Charlie for assistance in the field. Access and support to work at the Old Crow sites was facilitated by the Heritage Department of the Vuntut Gwitchin Government. This work used the Vincent J. Coates Genomics Sequencing Laboratory at University of California, Berkeley, supported by NIH S10 Instrumentation Grants S10RR029668 and S10RR027303. Support was provided from Yukon Heritage Branch; Natural Resources Canada Polar Continental Shelf Program (D.F.), Canada Research Chairs program, and Natural Sciences and Engineering Research Council (D.F.); National Science Foundation ARC-09090456 and ARC-1417046, and Gordon and Betty Moore Foundation GBMF3804 (to B.S.); and Australian Research Council DP0878604 and FT130100195 (to L.J.A.).

- Knapp AK, et al. (1999) The keystone role of bison in North American tallgrass prairie. *Bioscience* 49:39–50.
- Guthrie RD (1970) Bison evolution and zoogeography in North America during the Pleistocene. *Q Rev Biol* 45(1):1–15.
- Shapiro B, et al. (2004) Rise and fall of the Beringian steppe bison. *Science* 306(5701):1561–1565.
- Frisen GC (1978) *Prehistoric Hunters of the High Plains* (Academic, New York).
- Freeze CH, et al. (2007) Second chance for the plains bison. *Biol Conserv* 136:175–184.
- MacFadden BJ (1988) Horses, the fossil record, and evolution. *Evolutionary Biology*, eds Hecht MK, Wallace B, Prance GT (Springer, New York), Vol 22, pp 131–158.
- Lister AM, Sher AV (2015) Evolution and dispersal of mammoths across the Northern Hemisphere. *Science* 350(6262):805–809.
- Bell CJ, et al. (2004) The North American Pliocene and Pleistocene sequences. *Cenozoic Mammals of North America*, ed Woodburne MO (Univ of California Press, Berkeley).
- Savage DE (1951) Late Cenozoic vertebrates of the San Francisco Bay region, California. *Publ Depart Geol Sci* 28:1–30.
- Barnosky AD, et al. (2014) Prelude to the Anthropocene: Two new North American land mammal ages (NALMAs). *Anthropol Rev* 1:225–242.
- McDonald JN, Morgan GS (1999) The appearance of bison in North America. *Curr Res Pleist* 16:127–129.
- Péwé TL (1975) *Quaternary Geology of Alaska*, USGS Professional Paper 835 (US Government Print Office, Washington, DC), Vol 835.
- Hamilton TD, Craig JL, Sellman PV (1988) The Fox permafrost tunnel: A Late Quaternary geologic record in central Alaska. *GSA Bull* 100:948–969.
- Preece SJ, Westgate JA, Stemper BA, Pewe TL (1999) Tephrochronology of late Cenozoic loess at Fairbanks, central Alaska. *GSA Bull* 111:71–90.
- Sanders AE, Weems RE, Albright LB, III (2009) Formalization of the Middle Pleistocene 'Ten Mile Hill Beds' in South Carolina with evidence for placement of the Irvingtonian-Rancholabrean boundary. *Papers on Geology, Vertebrate Paleontology, and Biostratigraphy in Honor of Michael O. Woodburne*, ed Albright, III LB (Museum of Northern Arizona, Flagstaff, AZ), Vol 65, pp 363–370.
- Szabo BJ (1985) Uranium-series dating of fossil corals from marine sediments of southeastern United States Atlantic Coastal Plain. *GSA Bull* 96:398–406.
- Hollin JT, Hearty PJ (1990) South Carolina interglacial sites and stage 5 sea levels. *Quat Res* 33:1–17.
- Bell CJ, Repenning CA (1999) Observations on dental variation in *Microtus* from the Cudahy Ash Pit Fauna, Meade County, Kansas and implications for Irvingtonian microtine rodent biochronology. *J Vert Paleontol* 19:757–766.
- Schultz CB, Martin LD (1977) Biostratigraphy of the Neogene-Quaternary boundary in North America. Proceedings of the 2nd Symposium of the Neogene-Quaternary Boundary, Bologna. *G Geol* XLI:285–295.
- Forman SL, Pierson J (2002) Late Pleistocene luminescence chronology of loess deposition in the Missouri and Mississippi river valleys, United States. *Paleo3* 186:25–46.
- Orlando L, et al. (2013) Recalibrating *Equus* evolution using the genome sequence of an early Middle Pleistocene horse. *Nature* 499(7456):74–78.
- Storer JE (2004) A Middle Pleistocene (late Irvingtonian) Mammalian fauna from Thistle Creek, Klondike Goldfields Region of Yukon Territory, Canada. *Paludicola* 4:115–155.
- Westgate JA, et al. (2008) Changing ideas on the identity and stratigraphic significance of the Sheep Creek tephra beds in Alaska and the Yukon Territory, northwestern North America. *Quat Int* 178:183–209.
- Miller IM, et al. (2014) Summary of the Snowmastodon Project Special Volume: A high-elevation, multi-proxy biotic and environmental record of MIS 6–4 from the Ziegler Reservoir fossil site, Snowmass Village, Colorado, USA. *Quat Res* 82:618–634.
- Pinsof JD (1998) The American Falls local fauna: Late Pleistocene (Sangamonian) Vertebrates from Southeastern Idaho. *And Whereas...: Papers on the Vertebrate Paleontology of Idaho Honoring John A. White, Volume 1., Occasional Paper 36*, eds Akersten WA, McDonald HG, Meldrum DJ, Flint MEJ (Idaho Museum of Natural History, Pocatello, ID.) pp 121–145.
- Drummond A, Rodrigo AG (2000) Reconstructing genealogies of serial samples under the assumption of a molecular clock using serial-sample UPGMA. *Mol Biol Evol* 17(12):1807–1815.
- Jopling AV, Irving WN, Beebe BF (1981) Stratigraphic, sedimentological and faunal evidence for the occurrence of pre-Sangamonian artefacts in northern Yukon. *Arctic* 34:3–33.
- Kuzmina S, Froese DG, Jensen BJL, Hall E, Zazula GD (2014) Middle Pleistocene (MIS 7) to Holocene fossil insect assemblages from the Old Crow basin, northern Yukon, Canada. *Quat Int* 341:216–242.
- Preece S, et al. (2011) Old Crow tephra across eastern Beringia: A single cataclysmic eruption at the close of Marine Isotope Stage 6. *Quat Sci Rev* 30:2069–2090.
- Reyes AV, Froese DG, Jensen BJL (2010) Permafrost response to last interglacial warming: Field evidence from non-glaciated Yukon and Alaska. *Quat Sci Rev* 29:3256–3274.
- Matthews JV, Jr, Schweger CE, Janssens JA (1990) The last (Koy-Yukon) interglaciation in the northern Yukon: Evidence from Unit 4 at Ch'j'ee's Bluff, Bluefish Basin. *Geogr Phys Quat* 44:341–362.
- Shapiro B, Hofreiter M (2014) A paleogenomic perspective on evolution and gene function: New insights from ancient DNA. *Science* 343(6169):1236573.
- Douglas KC, et al. (2011) Complete mitochondrial DNA sequence analysis of Bison bison and bison-cattle hybrids: Function and phylogeny. *Mitochondrion* 11(1):166–175.

34. Achilli A, et al. (2008) Mitochondrial genomes of extinct aurochs survive in domestic cattle. *Curr Biol* 18(4):R157–R158.
35. Kirillova IV, et al. (2015) An ancient bison from the mouth of the Rauchua River (Chukotka, Russia). *Quat Res* 84:232–245.
36. Hu A, et al. (2010) Influence of Bering Strait flow and North Atlantic circulation on glacial sea-level changes. *Nat Geosci* 3:118–121.
37. Vaelbroeck C, et al. (2002) Sea-level and deep water temperature changes derived from benthic foraminifera isotopic records. *Quat Sci Rev* 21:295–305.
38. Reyes AV, et al. (2010) A late-Middle Pleistocene (Marine Isotope Stage 6) vegetated surface buried by Old Crow tephra at the Palisades, interior Alaska. *Quat Sci Rev* 29: 801–811.
39. Aitken MJ (1998) *An Introduction to Optical Dating: The Dating of Quaternary Sediments by the Use of Photon-Stimulated Luminescence* (Oxford Univ Press, Oxford).
40. Arnold LJ, Demuro M, Navazo Ruiz M, Benito-Calvo A, Pérez-González A (2013) OSL dating of the Middle Palaeolithic Hotel California site, Sierra de Atapuerca, north-central Spain. *Boreas* 42:285–305.
41. Arnold LJ, Demuro M, Navazo Ruiz M (2012) Empirical insights into multi-grain averaging effects from 'pseudo' single-grain OSL measurements. *Radiat Meas* 47:652–658.
42. Arnold LJ, Roberts RG (2009) Stochastic calculation of multi-grain equivalent dose (De) distributions: Implications for OSL dating of sediment mixtures. *Quat Geochronol* 4:204–230.
43. Galbraith RF, Roberts RG, Laslett GM, Yoshida H, Olley JM (1999) Optical dating of single and multiple grains of quartz from Jinmium rock shelter, northern Australia: Part I, experimental design and statistical models. *Archaeometry* 41:339–364.
44. Dabney J, et al. (2013) Complete mitochondrial genome sequence of a Middle Pleistocene cave bear reconstructed from ultrashort DNA fragments. *Proc Natl Acad Sci USA* 110(39):15758–15763.
45. Rohland N, Siedel H, Hofreiter M (2010) A rapid column-based ancient DNA extraction method for increased sample throughput. *Mol Ecol Resour* 10(4):677–683.
46. Meyer M, Kircher M (2010) Illumina sequencing library preparation for highly multiplexed target capture and sequencing. *Cold Spring Harbor Protoc* 2010(6):pdb.p05448.
47. Gansauge MT, Meyer M (2013) Single-stranded DNA library preparation for the sequencing of ancient or damaged DNA. *Nat Protoc* 8(4):737–748.
48. Slon V, et al. (2016) Mammalian mitochondrial capture, a tool for rapid screening of DNA preservation in faunal and undiagnostic remains, and its application to Middle Pleistocene specimens from Qesem Cave (Israel). *Quat Int* 398:210–218.
49. Li H, Durbin R (2009) Fast and accurate short read alignment with Burrows-Wheeler transform. *Bioinformatics* 25(14):1754–1760.
50. Briggs AW, et al. (2009) Targeted retrieval and analysis of five Neandertal mtDNA genomes. *Science* 325(5938):318–321.
51. Meyer M, et al. (2014) A mitochondrial genome sequence of a hominin from Sima de los Huesos. *Nature* 505(7483):403–406.
52. Jónsson H, Ginolhac A, Schubert M, Johnson PL, Orlando L (2013) mapDamage2.0: Fast approximate Bayesian estimates of ancient DNA damage parameters. *Bioinformatics* 29(13):1682–1684.
53. Lanfear R, Calcott B, Ho SYW, Guindon S (2012) Partitionfinder: Combined selection of partitioning schemes and substitution models for phylogenetic analyses. *Mol Biol Evol* 29(6):1695–1701.
54. Drummond AJ, Suchard MA, Xie D, Rambaut A (2012) Bayesian phylogenetics with BEAUti and the BEAST 1.7. *Mol Biol Evol* 29(8):1969–1973.
55. Gill MS, et al. (2013) Improving Bayesian population dynamics inference: A coalescent-based model for multiple loci. *Mol Biol Evol* 30(3):713–724.
56. Shapiro B, et al. (2011) A Bayesian phylogenetic method to estimate unknown sequence ages. *Mol Biol Evol* 28(2):879–887.
57. Guthrie RD (1990) *Frozen Fauna of the Mammoth Steppe* (Univ of Chicago Press, Chicago, IL).
58. Skinner MF, Kaisen OC (1947) The fossil bison of Alaska and preliminary revision of the genus. *Bull Am Mus Nat Hist* 89:123–256.
59. Berger GW (2003) Luminescence chronology of late Pleistocene loess-paleosol and tephra sequences near Fairbanks, Alaska. *Quat Res* 60:70–83.
60. Audclair M, Lamothe M, Lagroix F, Banerjee SK (2007) Luminescence investigation of loess and tephra from Halfway House section, Central Alaska. *Quat Geochronol* 2:34–38.
61. Péwé TL, Berger GW, Westgate JA, Brown PM, Leavitt SW (1997) Eva Interglaciation Forest Bed, unglaciated east-central Alaska: Global warming 125,000 years ago. *GSA Special Publication*.
62. Hamilton TD, Brigham-Grette J (1991) The last interglaciation in Alaska: Stratigraphy and paleoecology of potential sites. *Quat Int* 10-12(C):49–71.
63. Mathews P, Begét J, Mason O, Gelvin-Reymiller C (2003) Late Pliocene to late Pleistocene environments preserved at the Palisades Site, central Yukon River, Alaska. *Quat Res* 60:33–43.
64. McDowell PF, Edwards ME (2001) Evidence of Quaternary climatic variations in a sequence of loess and related deposits at Birch Creek, Alaska: Implications for the stage 5 climatic chronology. *Quat Sci Rev* 20:63–76.
65. Hughes OL, et al. (1981) Upper Pleistocene stratigraphy, paleoecology and archeology of northern Yukon interior, eastern Beringia 1. Bonnet Plume Basin. *Arctic* 34:329–365.
66. Harington CR (2011) Pleistocene vertebrates of the Yukon Territory. *Quat Sci Rev* 30: 2341–2354.
67. Schweger CE (1989) The Old Crow and Bluefish basin, Northern Yukon: development of the Quaternary history. *Late Cenozoic History of the Interior Basins of Alaska and the Yukon*, eds Carter DL, Hamilton TD, Galloway, JP (US Geological Survey, Washington, DC) pp 30–33.
68. Kennedy KE, Froese DG, Zazula GD, Lauriol B (2010) Last Glacial Maximum age for the northwest Laurentide maximum from the Eagle River spillway and delta complex, northern Yukon. *Quat Sci Rev* 29:1288–1300.
69. Zazula GD, Duk-Rodkin A, Schweger CE, Morlan RE (2004) Late Pleistocene chronology of glacial Lake Old Crow and the north-west margin of the Laurentide Ice Sheet. *Quaternary Glaciations - Extent and Chronology, Part II*. (Elsevier, Amsterdam) pp 347–362.
70. Murray AS, Wintle AG (2000) Luminescence dating of quartz using an improved single-aliquot regenerative-dose procedure. *Radiat Meas* 32:57–73.
71. Arnold LJ, et al. (2011) Paper II—Dirt, dates and DNA: OSL and radiocarbon chronologies of perennally frozen sediments in Siberia, and their implications for sedimentary ancient DNA studies. *Boreas* 40:417–445.
72. Jacobs Z, Duller GAT, Wintle AG (2006) Interpretation of single-grain De distributions and calculation of De. *Radiat Meas* 41:264–277.
73. Yoshida H, Roberts RG, Olley JM, Laslett GM, Galbraith RF (2000) Extending the age range of optical dating using single 'supergrains' of quartz. *Radiat Meas* 32:439–446.
74. Wintle AG, Murray AS (2006) A review of quartz optically stimulated luminescence characteristics and their relevance in single-aliquot regeneration dating protocols. *Radiat Meas* 41:369–391.
75. Arnold LJ, Roberts RG (2011) Paper I—Optically stimulated luminescence (OSL) dating of perennally frozen deposits in north-central Siberia: OSL characteristics of quartz grains and methodological considerations regarding their suitability for dating. *Boreas* 40:389–416.
76. Arnold LJ, Roberts RG, Galbraith RF, DeLong SB (2009) A revised burial dose estimation procedure for optical dating of young and modern-age sediments. *Quat Geochronol* 4:306–325.
77. Galbraith RF, Green PF (1990) Estimating the component ages in a finite mixture. *Nucl Tracks Radiat Meas* 17:197–206.
78. Lisiecki LE, Raymo ME (2005) A Pliocene-Pleistocene stack of 57 globally distributed benthic $\delta^{18}O$ records. *Paleoceanography* 20:PA1003.
79. Morlan RE (1989) Paleoeological implications of Late Pleistocene and Holocene microtine rodents from the Bluefish Caves, northern Yukon Territory. *Can J Earth Sci* 26:149–156.
80. Harington CR (2003) *Annotated Bibliography of Quaternary Vertebrates of Northern North America—With Radiocarbon Dates* (Univ of Toronto Press, Toronto), p 360.
81. Weinstock J, et al. (2005) Evolution, systematics, and phylogeography of pleistocene horses in the new world: A molecular perspective. *PLoS Biol* 3(8):e241.
82. McDonald HG, Harington CR, de Iulius G (2000) The ground sloth *Megalonyx* from Pleistocene deposits of the Old Crow Basin, Yukon, Canada. *Arctic* 53:213–220.
83. Hoganson J, McDonald HG (2007) First report of Jefferson's ground sloth (*Megalonyx jeffersonii*) in North Dakota: Paleobiogeographical and paleoecological significance. *J Mammal* 88:73–80.
84. Harington CR (1989) Soergelia: An indicator of Holarctic Middle Pleistocene deposits. Second Annual Muskox Symposium (NRC Canada, Ottawa), pp A1–A9.
85. Hughes OL (1972) *Surficial geology of northern Yukon Territory and northwestern District of Mackenzie, Northwest Territories*, Geological Survey of Canada, Paper, (Geological Survey of Canada, Ottawa) Vol 69-36, pp 1–11.
86. Reyes AV, Zazula GD, Kuzmina S, Ager TA, Froese DG (2011) Identification of last interglacial deposits in eastern Beringia: A cautionary note from the Palisades, interior Alaska. *J Quat Sci* 26:345–352.
87. Fulton TL (2012) Setting up an ancient DNA laboratory. *Methods Mol Biol* 840:1–11.
88. Heintzman PD, et al. (2015) Genomic data from extinct North American *Camelops* revise camel evolutionary history. *Mol Biol Evol* 32(9):2433–2440.
89. Pigati JS, et al. (2014) Geologic setting and stratigraphy of the Ziegler Reservoir fossil site, Snowmass Village, Colorado. *Quat Res* 82:477–489.
90. Mahan SA, et al. (2014) A geochronologic framework for the Ziegler Reservoir fossil site, Snowmass Village, Colorado. *Quat Res* 82:490–503.
91. Kircher M, Sawyer S, Meyer M (2012) Double indexing overcomes inaccuracies in multiplex sequencing on the Illumina platform. *Nucleic Acids Res* 40(1):e3.
92. Maricic T, Whitten M, Pääbo S (2010) Multiplexed DNA sequence capture of mitochondrial genomes using PCR products. *PLoS One* 5(11):e14004.
93. Renaud G, Stenzel U, Kelso J (2014) IeeHom: Adaptor trimming and merging for Illumina sequencing reads. *Nucleic Acids Res* 42(18):e141.
94. Meyer M, et al. (2012) A high-coverage genome sequence from an archaic Denisovan individual. *Science* 338(6104):222–226.
95. Dabney J, Meyer M, Pääbo S (2013) Ancient DNA damage. *Cold Spring Harb Perspect Biol* 5(7):1–7.
96. Briggs AW, et al. (2007) Patterns of damage in genomic DNA sequences from a Neandertal. *Proc Natl Acad Sci USA* 104(37):14616–14621.
97. Verkaar ELC, Nijman IJ, Beeke M, Hanekamp E, Lenstra JA (2004) Maternal and paternal lineages in cross-breeding bovine species. Has wisent a hybrid origin? *Mol Biol Evol* 21(7):1165–1170.
98. Heintzman PD, et al. (2016) Bison phylogeography constrains dispersal and viability of the Ice Free Corridor in western Canada. *Proc Natl Acad Sci USA* 113(29):8057–8063.
99. Duller GAT (2003) Distinguishing quartz and feldspar in single grain luminescence measurements. *Radiat Meas* 37:161–165.
100. Aitken MJ (1985) *Thermoluminescence Dating* (Academic, London).
101. Adamiec G, Aitken M (1998) Dose-rate conversion factors: update. *Anc TL* 16:37–50.
102. Stokes S, et al. (2003) Alternative chronologies for Late Quaternary (Last Interglacial–Holocene) deep sea sediments via optical dating of silt-sized quartz. *Quat Sci Rev* 22:925–941.
103. Brennan BJ (2003) Beta doses to spherical grains. *Radiat Meas* 37:299–303.
104. Prescott JR, Hutton JT (1994) Cosmic ray contributions to dose rates for luminescence and ESR dating: Large depths and long-term time variations. *Radiat Meas* 23:497–500.
105. Pawley SM, et al. (2008) Age limits on Middle Pleistocene glacial sediments from OSL dating, north Norfolk, UK. *Quat Sci Rev* 27:1363–1377.
106. Duller GAT (2007) Assessing the error on equivalent dose estimates derived from single aliquot regenerative dose measurements. *Anc TL* 25:15–24.

Supporting Information

Froese et al. 10.1073/pnas.1620754114

SI Text

Stratigraphic Information and Chronological Contexts of CRH 11 and Ch'ijee's Bluff.

Old Crow tephra. Chronology at Ch'ijee's Bluff and CRH 11 relies on identification of tephra in sediment exposures. Individual tephra are readily characterized geochemically and, when combined with other correlative indicators, such as stratigraphy or paleoecology, can provide isochronous stratigraphic markers across a region.

Old Crow tephra, a rhyolite, is one of the most prominent of the numerous tephra preserved in Late Cenozoic sediments of eastern Beringia. Old Crow tephra is found throughout Alaska and western Yukon, with an estimated eruptive volume of $\sim 200 \text{ km}^3$ (29). Old Crow tephra has an isothermal plateau glass fission-track age of $124 \pm 10 \text{ kyBP}$ (weighted-mean of four age determinations at 1σ) (29), which is consistent with independent thermoluminescence (59) and infrared-stimulated luminescence (60) ages on bracketing loess near Fairbanks, Alaska. Throughout its range of distribution, Old Crow tephra is present in relatively organic-poor, massive to crudely stratified silt, with paleoecological indicators for a cool climate at the time of deposition (29, 38). The tephra is up to 5 m below woody or peaty organic-rich silt, with pollen, plant, and insect macrofossil indicators for boreal forest conditions and climate as warm or warmer than present that is ascribed to the peak of the last interglaciation, MIS 5e (31, 61–64). These age determinations, together with regional stratigraphic and paleoecological data, are most indicative that the Old Crow tephra was deposited during late MIS 6 (29–31).

Old Crow tephra provides a robust chronostratigraphic marker horizon for this study: interglacial deposits below the tephra must predate MIS 5, whereas sediment above the tephra but below the prominent last interglacial wood-rich/peaty silt represents a relatively narrow time window during latest MIS 6. Because the bison fossil was recovered from this narrow context, we ascribe a latest MIS 6 age to it of $\sim 130 \text{ kyBP}$. This age falls within the 1σ error range of the Old Crow tephra of $124 \pm 10 \text{ kyBP}$ (29, 30).

Field identification of Old Crow tephra was confirmed by electron probe microanalysis of glass shard major element geochemistry (Fig. S1) (28, 30). Briefly, sieved glass separates were mounted in acrylic pucks and analyzed on a JEOL 8900 microprobe at University of Alberta by wavelength dispersive spectrometry. Analytical conditions were a beam diameter of $10 \mu\text{m}$, 15-keV accelerating voltage, and 6-nA beam current; secondary standards (Lipari obsidian and a reference sample of Old Crow tephra) were used for quality control and to minimize potential variation caused by differences in calibration and standardization between analytical sessions.

CRH 11.

Stratigraphy. CRH 11, on the left bank of the Old Crow River ($67^\circ 49' \text{ N}$, $139^\circ 51' \text{ W}$), is one of the classic localities for Quaternary paleontology in eastern Beringia (27, 65, 66). The bluff comprises $\sim 30 \text{ m}$ of silt and sand, locally organic-rich, as described over 3 d of fieldwork in 2008 (28). The lowermost $\sim 2 \text{ m}$ of massive sandy-silt are unconformably overlain by $\sim 15 \text{ m}$ of low-angle cross-bedded sand and local gravel, grading upward to laminated silt and sand with abundant plant litter, and finally massive sandy silt at $\sim 17 \text{ m}$ above river level. This unit is overlain by 3 m of massive sandy silt with ice-wedge casts and disseminated pods of Old Crow tephra (28). The tephra-bearing unit is overlain by $\sim 7 \text{ m}$ of stratified sand with periglacial structures and organic interbeds, capped by a 1-m-thick peat. The uppermost 3 m of sediment at

CRH 11 are stratified sand and silt with organic detritus, grading to dark gray clays associated with Glacial Lake Old Crow (67–69).

Chronology. Chronology for the CRH 11 site is based on the presence of the Old Crow tephra at 18 m above river level (28) and OSL dating of sands from the lower bone-bearing unit up to 3 m above river level. Because the Old Crow tephra marks latest MIS 6 time, the interglacial unit underlying the Old Crow tephra at CRH 11 is at least MIS 7 in age (28). To confirm this, we collected four samples for additional OSL dating of this underlying unit.

OSL sampling focused on a 1-m-thick sequence of alternating point bar and overbank flow deposits interbedded with well-preserved macro-organic horizons. Samples CRH 11-1 and CRH 11-3 were both taken from 10- to 20-cm-thick, finely bedded sand lenses found immediately beneath the bone-rich gravels. CRH 11-2 was taken 60 cm below CRH 11-1, from a 20-cm sand lens underlying a dense organic mat of woody macros and leaves. CRH 11-4 was collected 40 cm above CRH 11-1 from within a 10- to 15-cm-thick, laterally continuous, gray clay-silt unit capping the main bone-bearing gravels. OSL samples were collected from cleaned exposures using opaque PVC tubes and wrapped in light-proof bags for transportation and storage. In the laboratory, quartz grains of $125\text{--}180 \mu\text{m}$ and $180\text{--}212 \mu\text{m}$ diameter were extracted from the unilluminated centers of the PVC tube samples under safe (dim red) light conditions and prepared for burial dose estimation using standard procedures (39), including etching by 48% hydrofluoric acid for 40 min to remove the α -irradiated external layers.

Single-grain equivalent dose (D_e) values were determined using the experimental apparatus described by Arnold et al. (40), the single-aliquot regenerative-dose (SAR) procedure (70) shown in Table S1, and the SAR quality assurance criteria outlined in Arnold et al. (41). A preheat of 160°C for 10 s was used in the SAR procedure before measuring the natural, regenerative and test dose OSL signals. These preheating conditions yielded the most accurate measured-to-recovered dose ratios (1.01 ± 0.03) for $\sim 100 \text{ Gy}$ dose-recovery experiments performed on multigrain (~ 400 -grain) aliquots of sample CRH 11-1 (Fig. S2A). Replicate single-grain dose-recovery tests performed on CRH 11-1 using a higher administered dose ($\sim 315 \text{ Gy}$) yielded measured-to-recovered dose ratios consistent with unity (1.01 ± 0.03) (Fig. S2B) and relatively low levels of overdispersion ($11 \pm 6\%$), confirming the suitability of the chosen preheat conditions for high-dose single-grain D_e estimation.

Representative OSL decay curves and dose–response curves of grains that passed the SAR quality assurance criteria are shown in Fig. S3. Grains accepted for D_e analysis typically displayed sensitivity-corrected natural test-dose (T_n) signals of $\sim 200\text{--}300 \text{ counts}/0.17 \text{ s}$ (Fig. 3), although a small population of grains displayed T_n signal intensities of $>500 \text{ counts}/0.17 \text{ s}$ (Fig. S3A). The majority of accepted grains display rapidly decaying OSL curves (reaching background levels within 0.4 s), which are consistent with quartz signals dominated by the most readily bleachable (so-called “fast”) OSL component. The single-grain dose–response curves are generally well represented by either a single saturating exponential function or a saturating exponential plus linear function, as has been widely reported for quartz grains with fast-dominated OSL signals (e.g., refs. 71–73). A significant proportion of grains resemble the class I “supergrains” of Yoshida et al. (73) and display very high characteristic saturation dose (D_0) values of $150\text{--}400 \text{ Gy}$ (Fig. S3) when fitted with a saturating exponential dose–response function. These

favorable dose-saturation properties have enabled us to obtain higher than average D_e values for these samples. Grains displaying continued linear growth at high doses also provided the opportunity to calculate finite D_e estimates with reasonable fitting uncertainties beyond the $2D_0$ practical limit of precise D_e interpolation suggested by Wintle and Murray (74).

Environmental dose rates were calculated using a combination of in situ FGS, HRGS, and ICP-MS, as detailed in Table S2. HRGS was performed on one of the samples (CRH 11-1) to assess the present-day state of secular (dis)equilibrium in the ^{238}U and ^{232}Th decay series of these sediments. The ratios of $^{226}\text{Ra}/^{238}\text{U}$, $^{210}\text{Pb}/^{226}\text{Ra}$, and $^{228}\text{Th}/^{228}\text{Ra}$ were 1.06 ± 0.05 , 1.03 ± 0.06 , and 0.98 ± 0.02 , respectively, for this sample. These parent-daughter ratios are all within unity at 1σ or 2σ , indicating that a condition of secular equilibrium currently exists in the ^{238}U and ^{232}Th decay series.

The four samples share broadly similar single-grain D_e distribution characteristics (Fig. S4). The D_e datasets cover wide ranges of dose values (relative D_e range = 1.6–1.7), they are each consistent with a single dose population centered on the weighted mean D_e value (as indicated by the large proportions of grains lying within the gray bands in Fig. S4), and they are not significantly skewed at the 95% confidence interval when assessed using a log weighted skewness test (42, 75). These D_e distributions also display relatively low overdispersion values of 11–20% (Table S2), similar to the values of $\leq 20\%$ reported for ideal, well-bleached single-grain samples that have not been affected by postdepositional mixing or β -dose spatial heterogeneity (e.g., ref. 42). These D_e distribution properties suggest that dose dispersion originating from extrinsic, field-related sources (e.g., partial bleaching, sediment mixing, β -dose heterogeneity) are relatively unimportant in relation to the size of the D_e measurement uncertainties. This interpretation is consistent with the sedimentological properties of these deposits (i.e., they comprise well-sorted sands and silts with clearly preserved primary sedimentary structures and boundaries). The broad range of D_e values obtained for the CRH 11 samples seems to be attributable to intrinsic, rather than external, sources of dose dispersion (i.e., scatter originating primarily from the experimental procedures themselves, particularly grain-to-grain variations in luminescence responses to the SAR conditions or the use of nonidentical field and laboratory bleaching/heating/irradiation conditions). This is borne out by the single-grain dose-recovery D_e dataset, which displays the same relative spread of values (dose-recovery relative D_e range = 1.6) as the natural D_e distributions and a consistent overdispersion value at 1σ ($11 \pm 6\%$). These similarities suggest that the specific sources of intrinsic D_e scatter captured by the dose-recovery test likely account for the natural D_e distribution characteristics of the CRH 11 samples.

In light of the aforementioned considerations, we have estimated the final burial doses of these samples from their weighted mean D_e estimates, calculated using the central age model (CAM) of Galbraith et al. (43). This choice of age model is also well-supported by the statistical criterion outlined by Arnold et al. (76); in all cases, the CAM yields a maximum log likelihood score (L_{max}) that is statistically indistinguishable from that obtained using alternative age models with additional parameters [e.g., the minimum age models of Galbraith et al. (43) or the finite mixture model of Galbraith and Green (77)].

The single-grain OSL ages for the CRH 11 samples are in correct stratigraphic order and are statistically indistinguishable at 1σ (Table S2). The weighted mean OSL age for the lowest bone-bearing units (208 ± 6 ka) indicates sediment deposition during MIS 7 (78), and is consistent with the presence of the 124 ± 10 -ka Old Crow tephra (29) in overlying deposits located ~ 18 m above the present-day river level at CRH 11. The reliability of the MIS 7 OSL age for the lowest bone-bearing units at CRH 11 is also supported by the presence of prominent woody

macro horizons within the dated fluvial sequence, which strongly indicate that interglacial rather than glacial conditions prevailed at the time of deposition.

Vertebrate fauna. We visited CRH 11 over a 3-d period (June 27–30, 2008) to sample the lowest bone-bearing unit, consisting of a series of thin gravel beds separated by gray clays about 3.5 m above the then-current water level. We exposed this unit along a 10-m front at the base of the bluff, focusing on visible bone. Most were retrieved at the interface between one of the gravel layers, 1- to 2-cm thick, and an overlying gray clay. This and other evidence suggests that the depositional setting was an aggrading point bar, along which bones and teeth carried along by currents were dropped, likely near the proximal end of the point bar. Immediately below the bone-bearing stratum was an extensive bed of organic matter, featuring well-preserved leaves and twigs in dense mats. Small concentrations of organic matter also occurred as lenses within the gravel/clay sequence.

In this section we briefly compare the material we recovered with the comprehensive faunal lists for the Old Crow Basin (OCB) compiled by Jopling et al. (27) in their table 2. Additional relevant notes on OCB fossil taxa may be found in Morlan (79) and references in Harington (80).

A total of 294 pieces recovered in the 2008 season were cataloged and incorporated into the collections of the Office of the Yukon Paleontologist. Virtually all of the pieces are fragments not readily assignable to species-level taxa. Isolated teeth were recovered, but these were rarely complete and often in very poor condition. This is consistent with the interpretation that the fossils were transported and rolled for a significant distance before final deposition on the point bar.

The list below consists of taxa positively recognized in this collection, together with Yukon Paleontology Program catalog numbers of representative elements (list is not exhaustive):

Mammuthus primigenius (319.0003, 0058, 0264: molar fragments). Although no complete teeth were found, the spacing between lamellae on some of the large molar fragments recovered suggests that *M. primigenius* is the mammoth species represented. Many of the numerous very large long bone fragments recovered are doubtlessly referable to this species as well.

Equus sp. (319.0015, 0068, 0277, 0280: molars and incisors). The taxonomy of the 40+ nominal species of *Equus* from Pleistocene North America is an unintelligible morass, all of the more so because ancient DNA evidence suggests that there may have been only one or two highly morphologically variable species in North America in the Late Pleistocene (81). In any case, no material diagnostic of any particular nominal species was recovered. Almost all horse teeth are split or otherwise damaged.

“Artiodactyl” (319.0257: astragalus). An artiodactyl astragalus too large to represent *Rangifer* may instead represent *Soergelia* or other ovibovin, although this cannot be affirmed in the absence of comparative material. This element has been sampled for ancient DNA purposes.

Rangifer tarandus (319.0282: premolar). Caribou is represented by isolated teeth and long bones.

Castoroides ohioensis (319.0189: incisor). Fragments of the distinctive, channeled incisors of this large beaver are well represented in the collection.

Castor canadensis (319.272: jaw). The much smaller living representative of *Castor* is definitively identified on the basis of a jaw fragment with distinctive p4 morphology.

“Rodent” (319.275; 319.271: incisor, tibia). A sliver of incisor enamel and a distal tibia, neither of which belong to either species of *Castor*, may represent at least one other big rodent (possibly *Ochotona ?whartoni*).

Gulo gulo (319.276: jaw). A left horizontal ramus with canine (broken) and P3 in situ. Measurements are close to those of extant wolverine and the fossil is therefore assigned to that species. This is the only definite carnivore element identified in the collection.

Megalonyx jeffersonii (319.013; jaw fragment). Although only the symphyseal area and an alveolus for the caniniform is preserved on this fossil, it is adequate for species determination. (There is little else this specimen could represent except another megalonychid sloth, and none is known from arctic North America except *M. jeffersonii*.) This element has been sampled for ancient DNA purposes.

Jopling et al. (27) concentrated on developing the biostratigraphy, and possible archeological significance, of four OCB localities, designated as OCR (= CRH of this paper) 11, 12, 15, and 300. In total, the authors listed 35 mammal taxa at reasonably low taxonomic levels (species or genus), in addition to 5 taxa of birds and 6 of fishes, organized into 7 “faunal assemblages” (FAs). Two thirds of the mammal species listed are rodents. The remainder include a small number of carnivores, all still extant, and several large herbivores, of which *Mammuthus*, *Equus verae*, and *Soergelia* sp. are extinct.

The FAs were grouped and tentatively dated by Jopling et al. (27) in their table 2 as “Latest Illinoian,” “?Sangamonian,” or “Early Wisconsinian,” depending on stratigraphic position and various age indicators. Although the total age range is reasonably large, the FAs are markedly oversplit, being largely defined by presence/absence of one or two supposed indicative species. Nevertheless, for convenience in reference the original FA designations are retained here.

The FAs of interest here, 1–4 in the Jopling et al. (27) scheme, are the oldest and occur in the stratigraphic layer denoted as Unit 1b at each of the four localities they studied. From section diagrams and descriptions provided in their paper, it is definite that our 2008 excavation took place in the same unit. FA 1 has the fewest listings, consisting of only three taxa at the species level, two of which are mammal (giant pika, *Ochotona* cf. *whartoni*, and giant beaver, *C. ohioensis*). The lists for FAs 3 and 4 are also species-poor, but include *Mammuthus*, *Equus*, and *Soergelia*. FA 2 presents a much longer list, covering 26 positively or tentatively identified mammal taxa, including mammoth and horse but not steppe muskox. *Bison* was not identified in any of the early FAs, consistent with our finding as well. However, Jopling et al. did not have independent chronology for the site when they worked there because the Old Crow tephra had not been noted by those authors. Their first record of bison is in FA 6 is an important observation (noted as possibly Sangamonian by the authors). Those fossils would have been above the Old Crow tephra in our stratigraphy and thus of MIS 5e (Sanagamonian age) or later in age. We recovered no in situ fossils at these levels in our excavations.

M. jeffersonii, long known from fossils collected from various positions along the Old Crow River (82), was unaccountably omitted by Jopling et al. (table 2 in ref. 27) in their taxon lists. We confirm the occurrence of this taxon in Unit 1b at CRH 11 on the basis of an edentulous partial mandible. McDonald et al. (82) and Hoganson and McDonald (83) regarded most, and perhaps all, occurrences of Jefferson’s ground sloth in arctic North America as Sangamonian, but with the new dating of CRH 11 it is clear that this xenarthran had previously occupied this area during MIS 7.

Soergelia, the steppe muskox, is widely accepted as a Middle Pleistocene taxon. Although we did not find any material certainly referable to this taxon, Harington (84) was aware of its possible biostratigraphic significance as a potential Middle Pleistocene marker (“Kansan” in his terminology).

Ch’ijee’s Bluff.

Stratigraphy and chronology. Ch’ijee’s Bluff (67° 29’ N, 139° 56’ W) is a prominent 4-km-long river exposure on the south bank of the Porcupine River, ~15 km downstream of the village of Old Crow in northern Yukon. The bluff is within the continuous permafrost zone (>90% perennially frozen ground by area), although permafrost at the site thawed during the last glaciation when the region was inundated by large glacial lakes or tectonically controlled pluvial lakes (68, 69). There is also stratigraphic evidence for thaw of near-surface permafrost during MIS 5e, the last interglaciation (30).

The bluff exposes ~50 m of unconsolidated Late Cenozoic sediment (Fig. 3) (31, 85). The lowermost third of the exposure comprises alluvial sand, silt, and gravel, with macrofossil and pollen biostratigraphy suggesting a Late Pliocene age. Massive and crudely laminated silt and clay, likely associated with Early or Middle Pleistocene lacustrine sedimentation, make up the middle third of the bluff.

The upper third of exposed sediment at Ch’ijee’s Bluff hosts the unit of interest for this study. This unit, termed Unit 4 by earlier workers (31, 85), is composed of massive and crudely laminated silt with locally organic-rich interbeds and laminae. The Old Crow tephra (29) is present in this unit across much of Ch’ijee’s Bluff (Fig. S3A). Pollen, insects, and plant macrofossils from sediments directly associated with Old Crow tephra indicate shrub-tundra habitat and cooler than present climate (31). The tephra is consistently stratigraphically below a prominent bed of dark-brown, macrofossil-rich organic silt that commonly includes large spruce (*Picea*) logs. Pollen, insects, and plant macrofossils from this organic bed are indicative of closed boreal forest warmer than the present climate (31); spruce pollen percentage is higher than present-day surface samples, and the assemblage includes several extralimital taxa that are currently only found well to the south (e.g., the beetles *Dyschirius laevifasciatus*, *Bradycellus lecontei*, and *Micropeplus sculptus*; abundant bark beetles from the family Scolytidae; trace pollen from *Typha*; and macrofossils of the plants *Carex sychnocephala*, *Chenopodium gigantospermum*, and *Sium suave*). Logs and organic detritus from the organic bed all have nonfinite ¹⁴C ages (30, 31), indicating that they are older than the ~50-ka limit of ¹⁴C dating and thus unlikely to be “young” organics placed into stratigraphic association with older sediments because of thaw slumping (86). Although Old Crow tephra is usually present 0.5–2 m below the organic bed, at some measured sections along Ch’ijee’s Bluff the organic bed truncates Old Crow tephra or grades into ice wedge casts that truncate the tephra, suggesting shallow ground thaw and associated sediment reworking (30). Collectively, at Ch’ijee’s Bluff and at other sites in eastern Beringia (38), the stratigraphic and paleoecological evidence indicate that Old Crow tephra was deposited late during the MIS 6 glacial, with the overlying organic bed representing warmer than present conditions during the last interglaciation (MIS 5e).

Bison at Ch’ijee’s Bluff. In July 2006, we discovered a partial bison metacarpal at Ch’ijee’s Bluff (Fig. 3C) (YG 264.1) near the downstream limit of exposed Old Crow tephra at the bluff. The tephra was 40-m above river level during a period of relatively low water levels. At this measured section, the laterally continuous Old Crow tephra is 1- to 10-cm-thick and undulates with 20–30 cm of relief. The tephra is hosted in massive silt with local organic interbeds. A 5- to 15-cm-thick organic-rich bed with abundant logs and twigs sharply overlies the silts that host Old Crow tephra; this sharp contact is 1.5–2.5 m above the tephra. The bison metacarpal was found in situ in the silts, ~125 cm above Old Crow tephra but several centimeters below the sharp contact with the woody organic-rich bed. Given the sharp contact between the tephra- and bone-bearing silt and the organic-rich bed, as well as the common occurrence of thaw-related unconformities associated with this sedimentary contact, the most parsimonious

interpretation of the stratigraphic setting (Fig. 3B) is that the bison fossil dates to latest MIS 6, immediately preceding the MIS 5e interglaciation.

Reconstructing the Mitogenomic Evolutionary History of North American Bison. To infer the evolutionary relationships among North American and Siberian bison, we performed phylogenetic analyses on a dataset of 46 bison and 4 yak mitochondrial genomes. This dataset comprised 10 present-day bison, one previously published Bison from Siberia, four previously published yaks, and 35 mitochondrial genomes that were isolated and assembled from Late Pleistocene and Holocene bison fossils as part of this study. Of these 35, 21 were not associated with either a radiocarbon date or stratigraphic information. We subsampled these and submitted them either to the KECK Accelerator Mass Spectrometry laboratory at the University of California (UC) Irvine or the Center for AMS (CAMS) at Lawrence Livermore National laboratory for ultrafiltered collagen extraction and radiocarbon dating. Sample details, ages, and GenBank accession numbers are provided in Dataset S1.

Mitochondrial genome reconstruction. We performed all molecular biology work before the library indexing PCR step in the dedicated ancient DNA clean room at the UC Santa Cruz Paleogenomics laboratory, following strict protocols for ancient DNA research (87), for all bison other than the giant long-horned bison from a site near Snowmass, Colorado.

We extracted DNA from 100 to 250 mg of powdered bone using either of two silica-based methods suitable for the recovery of highly fragmented DNA (44, 45). DNA was extracted from 12 of the bison fossils during previous studies (Dataset S1 and references therein). We then prepared and amplified DNA libraries using the Meyer and Kircher (46) protocol, as modified by Heintzman et al. (88), from all 34 of these DNA extracts. We enriched these libraries for molecules that were similar to the plains bison (*Bison bison*) reference mitochondrial genome (GenBank RefSeq: NC_012346.1) via hybridization capture using custom, in-solution, biotinylated, 120mer or 80mer RNA MYbaits probes (MYcroarray). Enrichment experiments followed the manufacturer's instructions (v1.3.8 or v2.3.1), with minimal modifications: the RNA baits were diluted 1:10 with 100 ng/ μ L yeast tRNA (Invitrogen) and we used the KAPA HiFi HotStart ReadyMix PCR kit (Kapa Biosystems) with a 30-cycle reaction, instead of the recommended 8–14 cycles, for the postenrichment amplification.

We sequenced the enriched libraries from both ends using either the Illumina MiSeq (UC Santa Cruz) or HiSeq-2000 (Vincent J. Coates Genomics Sequencing Laboratory at UC Berkeley) systems, for 2×75 or 2×150 cycles, respectively. We removed sequencing adapters and merged paired-end reads in SeqPrep (<https://github.com/jstjohn/SeqPrep>), with a minimum overlap of 10 bp required for reads to merge and discarded reads with a length shorter than 30 bp. We then mapped the merged and remaining unmerged reads to the *B. bison* reference mitochondrial genome using an iterative short-read assembler, MIA (50). To reduce the impact of DNA damage on the mitochondrial genome assembly, we only called consensus at each position where a minimum of three unique molecules mapped ($3\times$ coverage). If only three molecules mapped, all three had to be in agreement. Where more than three unique molecules mapped, we called a consensus at sites with at least 67% of called bases in agreement (51). Because mitochondria are haploid, this consensus-calling procedure, which takes into consideration the base quality score and the likelihood that a variant is the result of ancient DNA damage based on positional information in the molecule, provides an extremely robust means to determine consensus. Positions that did not meet these criteria were coded as missing data. This pipeline provided complete mitochondrial genome sequences for each library, with average coverage ranging

from $6.6\times$ to $898.4\times$ (Dataset S1), with $\sim 75\%$ of the samples having at least $20\times$ average coverage.

The giant long-horned bison (*Bison latifrons*) from Snowmass, Colorado. We obtained from the Denver Museum of Nature and Science a sample of the *B. latifrons* that was recovered from a recent excavation of the Ziegler Reservoir near Snowmass, Colorado (24). Snowmass is an ancient lake that formed at the top of a mountain ridge as glaciers retreated during the last part of MIS 6 (89). The chronology of the site has been established using a combination of radiocarbon and in situ cosmogenic ^{10}Be and ^{26}Al dates, uranium-series, and OSL dating (89, 90). We obtained a sample of a humerus of *B. latifrons* (DMNH EPV.67609), which was found in biostratigraphic zone 5d (BZ5d), and is associated with an age of 129 ± 10 to 113 ± 8 kyBP.

Because of its age and location of preservation, the Snowmass bison was, unsurprisingly, much more poorly preserved than the other bison fossils. We therefore used a highly sensitive approach to recover small fragments of DNA. In a dedicated ancient DNA clean room at the Max Planck Institute for Evolutionary Anthropology in Leipzig, Germany, we removed 50 mg of material using a sterile dentistry drill and extracted DNA following Dabney et al. (44). We then converted a fraction of the extract into a DNA library by single-stranded library preparation (47). We amplified and labeled the library with two sample-specific indices (91) and enriched for mitochondrial DNA in two rounds of bead-based hybridization capture (92), using a probe set that encompasses complete reference mitochondrial genome sequences from 242 eutherian mammal species, including *B. bison* (48). The enriched library was sequenced from both ends in a pool with other libraries on Illumina's MiSeq using a $76+7+76+7$ -cycles recipe for double-index sequencing (91). Reads perfectly matching the expected index combination were isolated and full-length molecule sequences were reconstructed by overlapping of paired-end reads (93). Merged sequences longer than 30 bp were aligned to the plains bison reference mitochondrial genome using BWA (49) with "ancient" parameters (94). Duplicates were removed by calling a consensus from sequences with identical alignment start and end coordinates using bam-rmdup (<https://bitbucket.org/ustenzel/biohazard>). In total, we obtained 2,927 unique sequences that mapped to the plains bison mitochondrial genome (Dataset S1). To obtain a draft mitochondrial consensus sequence of the specimen, we followed a procedure used recently for consensus calling from highly degraded ancient DNA (51). Briefly, a consensus base was called for positions covered by at least three sequences that were at least in 67% agreement. We further masked T nucleotides in the first five positions of each sequence to reduce the impact of miscoding DNA damage on consensus quality. With this procedure, we obtained consensus calls for 10,714 positions of the specimen's mitochondrial genome.

Assessment of mitochondrial DNA damage. We scrutinized the reads mapped to bison for patterns of DNA damage, which are expected in degraded specimens (95). In a subset of samples, we assessed DNA fragment length distributions and the rates of miscoding lesions at the 5' and 3' ends of the aligned reads. These samples included the Ch'jee's Bluff steppe and Snowmass bison, as well as four other steppe bison from either Siberia (AE006, AE010) or North America (MS220, PH027). For the five steppe bison, we mapped the merged and remaining unmerged reads from SeqPrep to each steppe bison's consensus sequence in BWA. This approach was to ensure that detected mismatches were not because of evolutionary divergence from the reference sequence. We analyzed damage patterns for each alignment using mapDamage v2.0.5 (52). For the Snowmass bison, we assessed DNA damage, using the unique reads aligned to the plains bison reference mitochondrial genome, in mapDamage.

The Ch'jee's Bluff and Snowmass bison samples display the shortest modal lengths (54 and 35 bp, respectively) (Fig.

S6 A–F), consistent with their great age. As expected from depurination-induced fragmentation, all six samples exhibit noticeable increases in purine frequencies at the base position immediately preceding or following the 5' and 3' ends of reads, respectively (95), with the Snowmass bison sample most prominently displaying these patterns. Finally, all samples exhibit excesses of cytosine to thymine misincorporations at the ends of reads, respectively, consistent with the presence of deamination-induced base damage (95, 96). The Ch'ijee's Bluff steppe bison sequences exhibit misincorporation rates similar to the other, younger steppe bison bone samples (Fig. S6 C, I, L, O, and R), whereas the Snowmass bison sequences display very strong accumulations of cytosine to thymine substitutions at their ends (70–73%) (Fig. S6F). We should caution that the damage pattern variability between samples is likely to be, at least in part, related to the diverse DNA extraction and library preparation methods used in this study.

Phylogenetic analysis. We constructed an alignment of 46 bison mitochondrial genomes by supplementing our dataset (Dataset S1) with previously published mitochondrial genomes from 10 present-day North American bison [GU946976–84 (33); EU177871 (34)] and a ~10,800-y-old bison from Rauchua River, Chukotka (KR350472) (35). As outgroup, we additionally included four yak (*Bos grunniens*; KJ463418, AY684273, KJ704989, KM233416) mitochondrial genome sequences, whose mitochondrial lineage is closer to ancient and modern North American bison than that of the European bison (*Bison bonasus*) (97). After aligning these sequences, which resulted in a 16,322-bp alignment, we created a second dataset in which we reduced the alignment to include only those positions where the base could be called with confidence for the Snowmass bison. This resulted in an alignment of 10,714 bp.

For both the full and reduced alignments, we extracted seven partitions containing the control region, 12S rRNA, 16S rRNA, concatenated tRNAs, and separate alignments for first, second, and third positions within the coding regions of the mitochondrial genome. We then used PartitionFinder v1.1.1 (53) to identify the simplest partitioning strategy that best represented the data and the best evolutionary model for each partition. For both alignments, PartitionFinder suggested four partitions: firstPositions+tRNAs+12S+16S (TrN+G for both alignments); secondPositions (HKY for the full alignment, HKY+I for the reduced alignment); thirdPositions (TrN+G for the full alignment, HKY+G for the reduced alignment), and the control region (HKY+I+G for both alignments).

We then performed genealogical inference using BEAST v1.8.3 (54), assuming the partitioning and evolutionary models described above. Because it allows sufficient flexibility to explore the coalescent history of the sequences included in this dataset, we assumed the skygrid coalescent prior (55) and the strict molecular

clock (with separate rates for each partition), which we calibrated using age of each bison from which data were available. Ages of Late Pleistocene and Holocene bison were the median calibrated radiocarbon age before present (Dataset S1). Ages of the Ch'ijee's Bluff and Snowmass bison were sampled from distributions (56). The age of the Ch'ijee's Bluff steppe bison was sampled from a normal prior with a mean of 125 kyBP and SD of 4.5 kyBP, to reflect that it was found in situ between the Old Crow tephra and the MIS 5e forest bed. The Snowmass bison was sampled from a normal prior with a mean of 124 kyBP and SD of 8.5 kyBP, to reflect that it was found in a layer associated with MIS 5d. We ran two Markov chain-Monte Carlo chains for 60 million iterations each, sampling trees and priors every 3,000 iterations. Log and tree files were visually inspected using Tracer v1.6 (tree.bio.ed.ac.uk/software/tracer). The first 10% of sampled states were discarded as burn-in, after which the two runs were combined. Trees were summarized and the maximum clade credibility tree identified using TreeAnnotator, which is distributed as part of the BEAST package. The maximum clade credibility tree was visualized and annotated in FigTree v1.4.2 (tree.bio.ed.ac.uk/software/figtree).

The two alignments produced nearly identical phylogenies, with higher support values at the nodes when the reduced alignment was used (Fig. S5). The timing of bison entry into North America (node 1 in Fig. 1E) is inferred to be 193–138 kyBP (reduced dataset) or 172–134 kyBP (full dataset). The mitochondrial phylogeny can be roughly divided into three well-supported clades with strong phylogeographic partitioning. Siberian bison (green lineages) cluster together in the most deeply diverging clade, within which we identify a second, strongly supported wave of bison dispersal into North America (node 2 in Fig. 1E). This second dispersal occurred during the period 45–21 kyBP (reduced dataset) or 36–21 kyBP (full dataset), broadly within MIS 3 or 2 (Fig. S5), during which the Bering Land Bridge was exposed (36). We note that although the second wave clade is poorly sampled in our dataset, and the timing may change slightly with additional samples, two waves of dispersal are clearly indicated by these data. Extant American bison mitochondrial diversity seems to be derived exclusively from the first wave of bison dispersal into North America (Fig. 1E and Fig. S5). We further note the single deeply diverging lineage from Rauchua River, Siberia, which was recently isolated from a well-preserved partial mummy dating to ~10.8 kyBP (35). Interestingly, this is the youngest Asian steppe bison from which mitochondrial data are available, and suggests that only a small subset of Asian diversity ever crossed the Bering Isthmus into North America. We do not find evidence for the migration of North American bison back into Asia, which tentatively suggests unidirectionality in Pleistocene bison migration across the Bering Land Bridge.

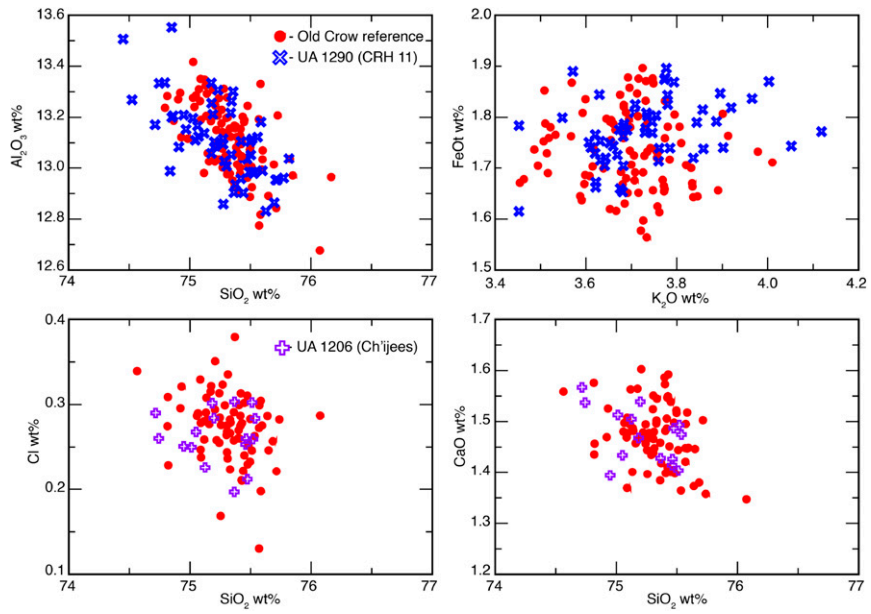


Fig. S1. Major element geochemistry of Old Crow tephra at CRH 11 and Ch'ijee's Bluff.

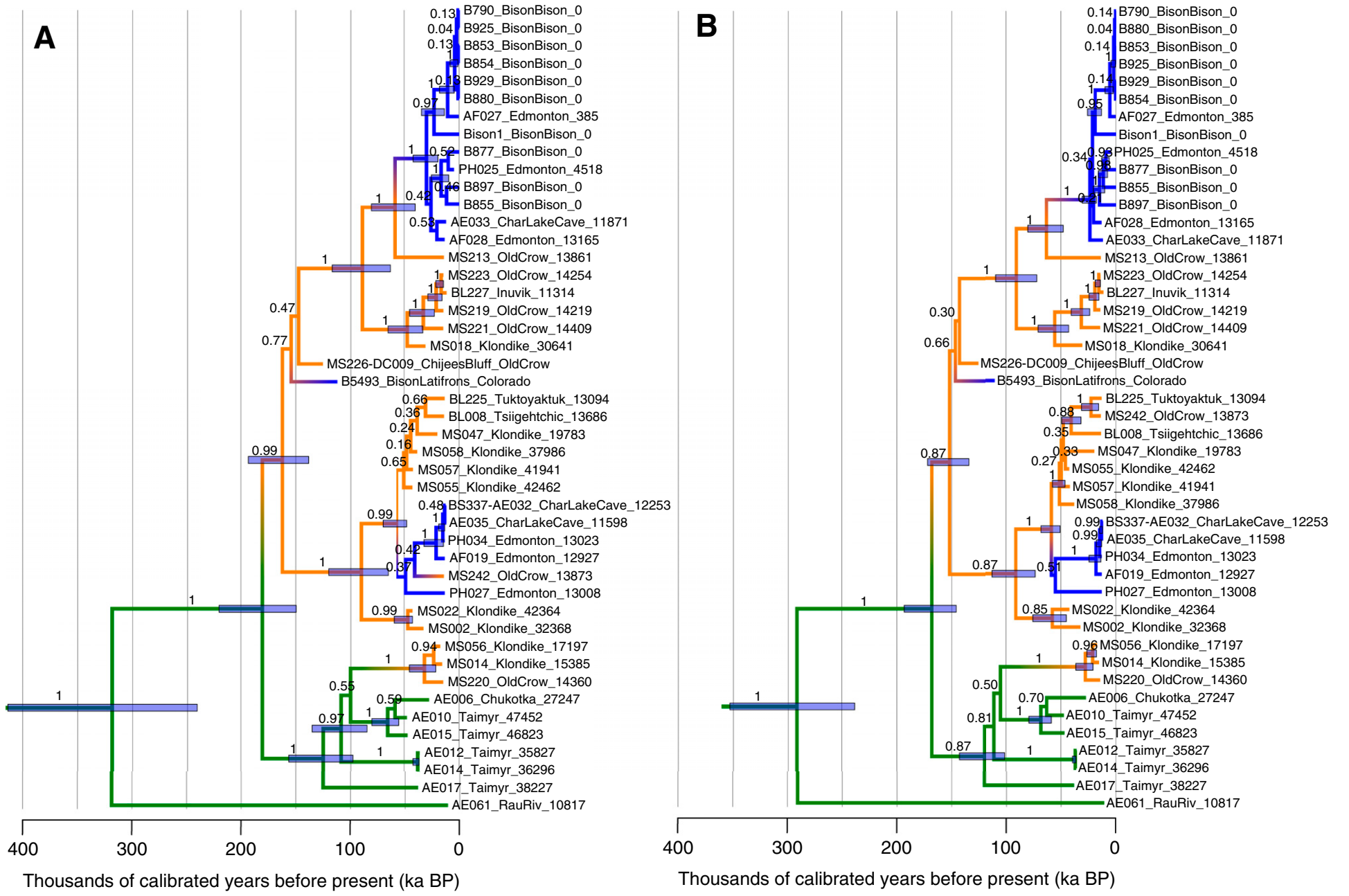


Fig. 55. Maximum clade credibility trees resulting from the Bayesian analysis of the reduced (A) and full (B) mitochondrial genome data sets. The reduced dataset (A) is also depicted in Fig. 1E. Colors are as in Fig. 1. Numbers along the branches are Bayesian posterior probability scores for each clade. Bars represent 95% highest posterior probability density intervals for node heights and are reported for nodes with a posterior probability score of >0.95 (A) or >0.85 (B). Tip labels follow the convention of sampleID_locality/species_age as in Dataset S1.

Table S1. SAR procedure used in this study

Step	Single-grain SAR Treatment	Signal/abbreviation
1	Dose (natural or laboratory)	D_n or D_x
2	Preheat (160 °C for 10 s)	PH ₁
3	Single-grain OSL stimulation (125 °C for 2 s)	L_n or L_x
4	Test dose	D_t
5*	IRSL stimulation (50 °C for 60 s)	—
6	Preheat (160 °C for 10 s)	PH ₂
7	Single-grain OSL stimulation (125 °C for 2 s)	T_n or T_x
8	Repeat SAR measurement cycle for different sized regenerative doses	—

Each of these SAR measurement cycles was repeated for the natural dose, four different sized regenerative doses and a 0 Gy regenerative-dose to measure OSL signal recuperation. Both the smallest and largest nonzero regenerative-dose cycles were repeated at the end of the SAR procedure to assess the suitability of the test dose sensitivity correction. The smallest regenerative-dose cycle was also repeated a second time with the inclusion of step 5 to check for the presence of feldspar contaminants using the OSL IR depletion ratio of Duller (99).

*Step 5 is only included in the single-grain SAR procedure when measuring the OSL IR depletion ratio (100).

Other Supporting Information Files

[Dataset S1 \(XLSX\)](#)

[Dataset S2 \(RTF\)](#)